

Highlights

A variationally consistent membrane wrinkling model based on tension-compression decomposition of the strain tensor*

Daobo Zhang, Josef Kiendl

- Research highlight 1 (A new variationally consistent membrane wrinkling model is proposed)
- Research highlight 2 (Great convergence behavior and straightforward implementation)
- Research highlight 3 (Residual stiffness for slackened state)

A variationally consistent membrane wrinkling model based on tension-compression decomposition of the strain tensor

Daobo Zhang^{a,*}, Josef Kiendl^a

^a*Institute of Engineering Mechanics and Structural Analysis - University of the Bundeswehr Munich, Werner-Heisenberg-Weg 39, 85579, Neubiberg, Germany*

Abstract

We propose a novel variationally consistent membrane wrinkling model for analyzing the mechanical responses of wrinkled thin membranes. The elastic strain energy density is split into tensile and compressive terms via a spectral decomposition of the strain tensor. Tensile and compressive parts of the stress and tangent material matrices are then obtained via consistent variation from the respective strain energies. Considering only the positive part of the strain energy in the variational formulation, we obtain a membrane with zero compressive stiffness. By adding the negative strain energy multiplied with a reduction factor, we further obtain a residual compressive stiffness, which improves stability and allows handling also states of slackening. Comparison with results from analytical, numerical and experimental examples from the literature on membrane wrinkling problems demonstrate the great performance and capability of the proposed approach, which is also compatible with commercial finite element software.

*Corresponding author.

Email address: `daobo.zhang@unibw.de` (Daobo Zhang)

Keywords:

Isogeometric analysis; Membrane; Wrinkling; Large deformation

1. Introduction

Wrinkling is a common occurrence observed in nonlinear elastic membrane structures, which bears significant relevance, as it can substantially affect their mechanical properties and performance. The investigation of wrinkling in thin membranes with diverse methods and techniques has been ongoing for several decades to enhance the understanding of their underlying characteristics. Despite extensive research, modeling and predicting the behavior of wrinkled membranes remains challenging. This is primarily because membranes exhibit minimal resistance to compression and bending. As a result, most compressive stresses within membranes are released through localized instability. It leads to out-of-plane displacements, which are typically referred to as wrinkles (Miyazaki, 2006).

Several analytical solutions have been developed to address membrane wrinkling issues, as evidenced by the works in Mansfield (1969), Reissner (1938), Wagner (1931), Wu (1978). These solutions are derived within the tension field theory (TFT) framework, a theoretical approach that describes the highly buckled or wrinkled state of membranes whose boundaries undergo certain in-plane displacements that exceed the critical thresholds necessary for initiating buckling phenomena. Notably, Stein and Hedgepeth (1961) derived a theory at small strains to predict the stresses and average deformations of partly wrinkled membranes by introducing an unknown function termed variable Poisson's ratio λ and vanishing one of the principal stresses in wrinkled regions. Additionally, they provided analytical solutions for various partly wrinkled membrane problems, commonly employed as benchmarks to validate the stresses predicted by newly developed methods. Other analyt-

ical approaches are mentioned for completeness, and those are based on a geometrically nonlinear Föppl-von Kármán theory (Cerda and Mahadevan, 2003, Puntel et al., 2011, Wong and Pellegrino, 2006b) and can depict the wrinkled configuration. However, these analytical solutions are often limited to specific problems and may lack applicability for cases that cannot be solved analytically. Therefore, numerical methods are preferred for analyzing wrinkled membrane problems, owing to their flexibility and ability to handle complex geometries and boundary conditions.

Previous numerical methods treating wrinkling in the finite element analysis framework can be broadly classified into two primary categories. This classification is determined by the requirement to obtain wrinkle details, including the number of wrinkles, wavelength, amplitude, wrinkle pattern, etc. The first relies on the buckling theory, which involves utilizing a highly dense mesh of shell elements with bending stiffness to resolve wrinkle details explicitly (Taylor et al., 2014, Wong and Pellegrino, 2006c). However, this method can be computationally expensive due to the need for a sufficiently refined mesh, and as pointed out in Jarasjarungkiat et al. (2008), the wrinkle length scale is frequently inconsistent with that of a finite element, leading to a mesh-dependent solution. In addition, a geometric imperfection must often be imposed on the membrane to induce wrinkles, which may also affect the results (Iwasa et al., 2004). Consequently, the costs of this approach can rapidly become prohibitive, thereby limiting its practicality. Other relevant studies refer to Flores and Oñate (2011), Fu et al. (2021), Verhelst et al. (2021), to name a few.

The second one is to use a coarse mesh of membrane elements embedded

with appropriate wrinkling models, mainly founded upon the assumptions of tension field theory (Steigmann, 1990). It assumes that the wrinkled membrane exhibits zero bending stiffness and cannot support compressive stress. Following the wrinkling process, the stress field within the wrinkled regions is presumed to be in a uniaxial tension stress state, whereby only one of the principal stress components is non-zero. Although the detailed wrinkles cannot be captured with these assumptions, it enables the identification of wrinkled regions and the directions of wrinkles, providing valuable insights into the overall behavior of the wrinkled membrane. Our work presented in this paper is carried out by following the second strategy. Thus, a literature review of wrinkling models is given below.

Most tension field theory-based wrinkling models can be broadly classified into two groups: kinematic modification methods and material modification methods. In general, the concept of the kinematic method is to modify the deformation gradient tensor by introducing additional parameters. Remarkably, the Roddeman model (Roddeman et al., 1987a,b) has garnered significant attention, which extends the earliest Wu model (Wu and Canfield, 1981) to anisotropic material by incorporating a virtual elongation in deformation tensor to satisfy uniaxial tension conditions. Among the subsequent developments of this model (Hornig and Schoop, 2003, Lu et al., 2001, Nakashino and Natori, 2006, 2005, Schoop et al., 2002), Nakashino and Natori (2005) circumvented the cumbersome linearization of the modified strain tensor to adjust the stress-strain tensor in the element level and recently Nakashino's model has been applied in isogeometric analysis (Nakashino et al., 2020). Other models, such as Miyazaki's model (Miyazaki, 2006), which incorporates

virtual elongation and shear deformation simultaneously into the deformation tensor, and direct modification of Green-Lagrange strain tensor (Kang and Im, 1997, 1999, Raible et al., 2005), can also be classified as kinematic modification methods.

Material modification methods, which modify the stress-strain relation, can be divided into four subcategories. The first class is to modify the material parameters. For instance, Miller and Hedgepeth (1982), Miller et al. (1985) extended the variable Poisson’s ratio concept (Stein and Hedgepeth, 1961) into finite element static analysis and proposed the iterative material properties (IMP) model, where the local elasticity matrix is iteratively revised according to the state of strain in a previous load increment. The second and third ones are to use penalization techniques (Contri and Schrefler, 1988, Jarasjarungkiat et al., 2008, Liu et al., 2001, Rossi et al., 2005, Woo et al., 2004), and projection matrices (Akita et al., 2007, Jarasjarungkiat et al., 2009, Le Meitour et al., 2021a) to eliminate compressive stresses by softening the constitutive tensor. However, the methods mentioned earlier require an explicit wrinkling criterion to evaluate the membrane states such as taut, wrinkled, and slack, as shown in Fig. 2. More details and discussions of choosing a wrinkling criterion are given in Rossi et al. (2005), Wang et al. (2014). This reliance may lead to convergence problems due to the sudden changes in the tangent stiffness matrix. Thus, these shortcomings have motivated the fourth approach based on Pipkin’s method, as documented in Epstein and Forcinito (2001), Haseganu and Steigmann (1994), Mosler (2008), Mosler and Cirak (2009), Pipkin (1986). In this method, the strain energy density is replaced by a relaxed energy density acquired through an

optimization procedure. Consequently, the stresses derived from the relaxed energy density are comparable to those obtained via the tension field theory. However, the inherent mathematical complexity and associated implementation challenges have resulted in a relative lack of attention to this concept in the literature. Hence, developing a new wrinkling model capable of dealing with these drawbacks and inconveniences is necessary.

In this paper, we propose a novel variationally consistent membrane wrinkling model based on the spectral decomposition of the strain tensor (Miehe et al., 2010) to improve convergence behavior and reduce implementation burdens. We split the strain tensor into positive and negative components based on their eigenvalues. It allows us to decompose the strain energy density additively into positive and negative contributions. Considering only the positive part of the strain energy in the variational formulation, we obtain a membrane with zero compressive stiffness. By adding the negative strain energy multiplied with a reduction factor, we further obtain a residual compressive stiffness, which improves stability and allows handling also states of slackening. Thereby, the strain-based wrinkling criterion can be self-adaptively satisfied without the reliance on if-else logical judgment in the implementation. It ensures the consistency of the wrinkling model and avoids many iterations triggered by a membrane state transition. The spectral decomposition also provides information on the wrinkling direction. We consistently derive the modified strain energy density with respect to the strain variable to determine the new stress and material tensor formulations. Finally, we incorporate our proposed wrinkling model into an isogeometric membrane element and verify its effectiveness with benchmark problems.

The paper is organized as follows. In Section 2, we provide an overview of the geometrical basics of the membrane description, the membrane kinematics, and its variational formulation. This section serves as the foundation for the subsequent sections. Section 3 presents the newly developed wrinkling model, which includes the spectral decomposition of the strain tensor and the consistent derivation of new stress and constitutive tensors. In addition, we briefly discuss the linearization of its variational formulation and isogeometric discretization in Section 4. In order to demonstrate the applicability of the presented methods, four tests are presented in Section 5, including benchmark examples from the literature with analytical, experimental, or numerical reference solutions. Finally, in Section 6, we summarize the key features of our proposed wrinkling model and suggest potential future directions for research in this area.

2. Membrane formulation

In this section, we present a concise overview of the fundamental aspects of the geometry, kinematics, and material law of a membrane. As shown in Fig. 1, a membrane can be generally represented as a curved surface with a certain thickness t , described by the position vector $\mathbf{x}(\theta^\alpha)$. The surface coordinates are denoted as θ^α . Greek indices take on values of $\{1, 2\}$, and the summation convention for repeated indices is employed. Then, the covariant base vectors \mathbf{g}_α on the midsurface in the current configuration are defined as:

$$\mathbf{g}_\alpha = \frac{\partial \mathbf{x}}{\partial \theta^\alpha} = \mathbf{x}_{,\alpha}. \quad (1)$$

Similarly, in the context of the reference configuration, the covariant basis vectors are denoted as \mathbf{G}_α . Then, the contravariant basis vectors \mathbf{G}^α and \mathbf{g}^α can be determined by the rule:

$$\mathbf{G}^\alpha \cdot \mathbf{G}_\beta = \delta_\beta^\alpha, \quad \mathbf{g}^\alpha \cdot \mathbf{g}_\beta = \delta_\beta^\alpha, \quad (2)$$

where δ_β^α is the Kronecker delta. If $\alpha = \beta$, $\delta_\beta^\alpha = 1$; otherwise, $\delta_\beta^\alpha = 0$. The metric coefficients of the midsurface in the reference configuration $G_{\alpha\beta}$ and current configuration $g_{\alpha\beta}$ are represented as:

$$G_{\alpha\beta} = \mathbf{G}_\alpha \cdot \mathbf{G}_\beta, \quad g_{\alpha\beta} = \mathbf{g}_\alpha \cdot \mathbf{g}_\beta. \quad (3)$$

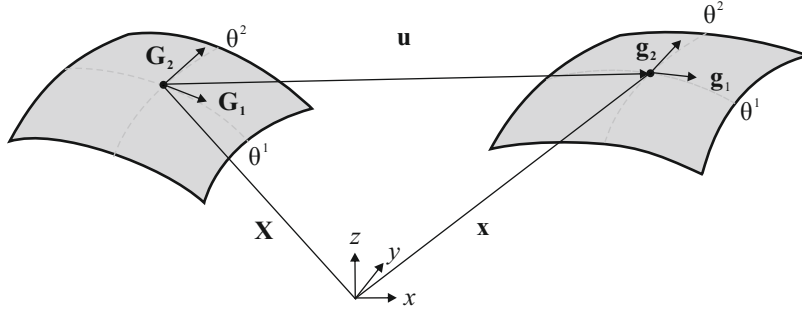


Figure 1: Schematic description of a membrane: \mathbf{X} and \mathbf{x} are the position vectors on the midsurface in the reference configuration and the deformed configuration with displacement vector \mathbf{u} , respectively.

Subsequently, the deformation gradient \mathbf{F} can be introduced and defined as:

$$\mathbf{F} = \mathbf{g}_\alpha \otimes \mathbf{G}^\alpha, \quad \mathbf{F}^T = \mathbf{G}_\alpha \otimes \mathbf{g}^\alpha. \quad (4)$$

In order to characterize the nonlinear relationship between deformations and strains, the Green-Lagrange strain tensor is employed and given by:

$$\mathbf{E} = \frac{1}{2} (\mathbf{F}^T \mathbf{F} - \mathbf{I}), \quad (5)$$

where \mathbf{I} denotes the identity tensor. The in-plane coefficients of \mathbf{E} are obtained by the metric coefficients in the deformed and undeformed configurations as:

$$E_{\alpha\beta} = \frac{1}{2} (g_{\alpha\beta} - G_{\alpha\beta}). \quad (6)$$

The second Piola-Kirchhoff (PK2) stress tensor \mathbf{S} is introduced as the energetically conjugate quantity to the Green-Lagrange strain tensor \mathbf{E} . It is derived from the strain energy density ψ with respect to the strain \mathbf{E} . Here, the strain energy density of the St.Venant-Kirchhoff constitutive model with plane stress is given by:

$$\psi(\mathbf{E}) = \frac{\lambda}{2} (\text{tr}(\mathbf{E}))^2 + \mu \text{tr}(\mathbf{E}^2) - \frac{\lambda^2}{2(\lambda + 2\mu)} (\text{tr}(\mathbf{E}))^2, \quad (7)$$

where λ is the first Lamé parameter and μ the second Lamé parameter, respectively. The stress tensor \mathbf{S} can be determined via the tangent material tensor \mathbb{C} and its coefficients $S^{\alpha\beta}$ are then expressed in terms of the material tensor coefficients $\mathbb{C}^{\alpha\beta\gamma\delta}$ as:

$$S^{\alpha\beta} = \mathbb{C}^{\alpha\beta\gamma\delta} E_{\gamma\delta}. \quad (8)$$

By approximating the differential volume dV as the product of the thickness t of membrane and its midsurface differential area dA , i.e., $dV \approx tdA$, the virtual work $\delta W(\mathbf{u}, \delta\mathbf{u})$ can be formulated as follows:

$$\delta W(\mathbf{u}, \delta\mathbf{u}) = \delta W^{\text{int}} - \delta W^{\text{ext}} = \int_A \mathbf{S} : \delta\mathbf{E} t \, dA - \int_A \mathbf{f} \cdot \delta\mathbf{u} \, dA, \quad (9)$$

which involves the internal virtual work δW^{int} and external virtual work δW^{ext} . Within the Eq. (9), $\delta\mathbf{E}$ represents the virtual strain, \mathbf{f} denotes the external force, and $\delta\mathbf{u}$ represents the virtual displacement.

3. New wrinkling model based on spectral decomposition

In this section, we present the new wrinkling model. The fundamental concept is to split the strain tensor \mathbf{E} into positive and negative components using its eigenvalues. Thus, the new wrinkling model categorizes the membrane wrinkling states as taut, wrinkled, or slackened, as shown in Fig. 2, following the principal strain-based criterion as:

$$\begin{aligned}
 E_{\min} > 0 &\Rightarrow \text{taut} \\
 E_{\max} > 0, \quad E_{\min} \leq 0 &\Rightarrow \text{wrinkled} . \\
 E_{\max} \leq 0 &\Rightarrow \text{slackened}
 \end{aligned}
 \tag{10}$$

Then, with the splitting of the strain tensor, the strain energy density can

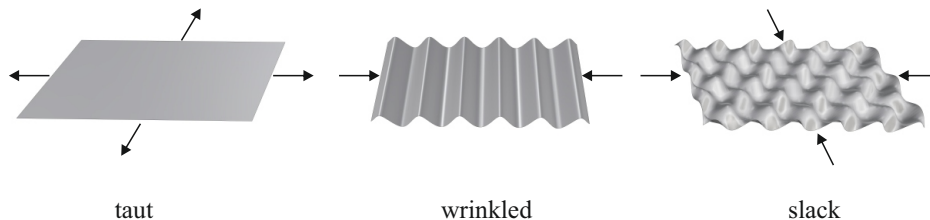


Figure 2: Wrinkling states: taut, wrinkled, slack

also be decomposed into positive and negative terms, allowing us to establish positive and negative stress and material tensor formulations. Furthermore, we incorporate a degradation factor into the decomposed strain energy to systematically adjust the impact arising from negative stress and its derived material tensor. Below, we provide the corresponding formulas and derivations.

Firstly, the strain tensor \mathbf{E} is spectrally decomposed into positive and negative parts to perform the splitting of the strain energy density and defined

as:

$$\mathbf{E} = E_\alpha \mathbf{n}_\alpha \otimes \mathbf{n}_\alpha = \mathbf{E}^+ + \mathbf{E}^-, \quad (11)$$

where E_α represents the eigenvalues (principal strains) corresponding to the eigenvectors \mathbf{n}_α (principal directions) of strain tensor \mathbf{E} . In the context of isotropic materials, the orthogonality of the eigenvectors makes them suitable for indicating the wrinkling directions (Jarasjarungkiat et al., 2008).

Remark 1. Due to the presence of the Poisson effect, accurately judging the states using the principal strain-based criterion can be challenging, as discussed in the literature (Liu et al., 2001, Wang et al., 2014). It would be physically more correct to work with the eigenvalues of the stress tensor, because it is theoretically possible to obtain positive minimum stress but negative minimum strain due to the Poisson effect. However, the numerical studies in Section 5 demonstrate that the strain-based model can give accurate results in a large variety of cases. The related works based on principal strain criterion are referred to Miller and Hedgepeth (1982), Miller et al. (1985).

The positive and negative strain tensors, denoted as \mathbf{E}^+ and \mathbf{E}^- , respectively, are then determined in terms of the positive and negative principal strains $\langle E_\alpha \rangle^\pm$ and formulated as follows:

$$\mathbf{E}^\pm = \langle E_\alpha \rangle^\pm \mathbf{n}_\alpha \otimes \mathbf{n}_\alpha, \quad (12)$$

with $\langle x \rangle^\pm = (x \pm |x|)/2$. Using the spectral decomposition of the strain tensor \mathbf{E} , the strain energy density $\psi(\mathbf{E})$ is expressed as a combination of positive and negative terms. This concept was used in Miehe et al. (2010) in

the context of phase-field fracture and was extended in Kiendl et al. (2016) to the case of plane stress problems. Thus, the positive and negative strain energy densities, denoted as $\psi^\pm(\mathbf{E})$, are given by:

$$\psi^\pm(\mathbf{E}) = \frac{\lambda}{2} (\langle \text{tr}(\mathbf{E}) \rangle^\pm)^2 + \mu \text{tr} \left((\mathbf{E}^\pm)^2 \right) - \frac{\lambda^2}{2(\lambda + 2\mu)} (\langle \text{tr}(\mathbf{E}) \rangle^\pm)^2. \quad (13)$$

In order to conform to the fact that a membrane can carry almost no compressive stresses, we introduce a scalar degradation factor $\eta \in [0, 1]$ to reduce the contribution of the negative strain energy density, leading to a minimization of compressive stresses in the wrinkling model. By doing so, the total strain energy density $\psi(\mathbf{E})$ is modified as:

$$\psi(\mathbf{E}) = \psi^+(\mathbf{E}) + \eta \psi^-(\mathbf{E}). \quad (14)$$

It is noteworthy that if the degradation factor was to be assigned a value of zero, it would result in the elimination of all contributions from the negative strain energy density $\psi^-(\mathbf{E})$. Consequently, this could not capture slacked states and would lead to convergence problems even in the case of temporary local slackening. To address this concern, we maintain a small non-zero value ($\eta = 10^{-4}$ in our work) for the degradation factor rather than setting it to zero completely.

Then, by taking the partial derivatives of the strain energy densities $\psi^+(\mathbf{E})$ and $\psi^-(\mathbf{E})$ with respect to the strain tensor \mathbf{E} , we can further decompose the stress tensor \mathbf{S} into positive and negative components:

$$\mathbf{S} = \frac{\partial \psi^+(\mathbf{E})}{\partial \mathbf{E}} + \eta \frac{\partial \psi^-(\mathbf{E})}{\partial \mathbf{E}} = \mathbf{S}^+ + \eta \mathbf{S}^-, \quad (15)$$

where the positive and negative stress tensors \mathbf{S}^\pm are given by:

$$\mathbf{S}^\pm = \frac{\partial \psi^\pm(\mathbf{E})}{\partial \mathbf{E}} = \lambda \langle \text{tr}(\mathbf{E}) \rangle^\pm \mathbf{I} + 2\mu \mathbf{E}^\pm - \frac{\lambda^2}{\lambda + 2\mu} \langle \text{tr}(\mathbf{E}) \rangle^\pm \mathbf{I}. \quad (16)$$

Subsequently, taking the partial derivative of Eq. (15) with respect to the strain tensor \mathbf{E} , the fourth-order constitutive tensor \mathbb{C} can be expressed as a combination of positive and negative components and is given by:

$$\mathbb{C} = \frac{\partial}{\partial \mathbf{E}} \left(\frac{\partial \psi^+(\mathbf{E})}{\partial \mathbf{E}} + \eta \frac{\partial \psi^-(\mathbf{E})}{\partial \mathbf{E}} \right) = \mathbb{C}^+ + \eta \mathbb{C}^-, \quad (17)$$

where \mathbb{C}^+ and \mathbb{C}^- correspond to the constitutive tensors associated with positive and negative strain energy densities, respectively. Their expressions are defined as:

$$\mathbb{C}^\pm = \frac{\partial}{\partial \mathbf{E}} \left(\left(\lambda - \frac{\lambda^2}{\lambda + 2\mu} \right) \langle \text{tr}(\mathbf{E}) \rangle^\pm \mathbf{I} + 2\mu \mathbf{E}^\pm \right). \quad (18)$$

For brevity, we separate the expression of the Eq. (18) in two terms. The partial derivative of the first term in Eq. (18) with respect to the strain tensor \mathbf{E} is carried out as:

$$\frac{\partial}{\partial \mathbf{E}} (\langle \text{tr}(\mathbf{E}) \rangle^\pm \mathbf{I}) = H(\pm \text{tr}(\mathbf{E})) \frac{\partial}{\partial \mathbf{E}} (\text{tr}(\mathbf{E}) \mathbf{I}), \quad (19)$$

where $H(x)$ is the Heaviside function. According to the work of Nilsen (2012), who was the first one showing the details of the derivation, a fourth-order tensor \mathbb{J} is introduced to define the derivative of the product of the trace of strain tensor $\text{tr}(\mathbf{E})$ and the identity tensor \mathbf{I} as:

$$\left(\frac{\partial}{\partial \mathbf{E}} (\text{tr}(\mathbf{E}) \mathbf{I}) \right)_{\alpha\beta\gamma\delta} := \mathbb{J} = \frac{\partial (\text{tr}(\mathbf{E}) \mathbf{I})_{\alpha\beta}}{\partial E_{\gamma\delta}} = \begin{cases} 0 & \text{if } \alpha \neq \beta \\ 0 & \text{if } \gamma \neq \delta \\ 1 & \text{if } \alpha = \beta \text{ and } \gamma = \delta \end{cases}. \quad (20)$$

Thereby, the Eq. (19) can be simply rewritten as:

$$\frac{\partial}{\partial \mathbf{E}} (\langle \text{tr}(\mathbf{E}) \rangle^\pm \mathbf{I}) = H(\pm \text{tr}(\mathbf{E})) \mathbb{J}. \quad (21)$$

Next, we address the partial derivative of the second term in Eq. (18), which involves the so-called projection operators \mathbb{P}_E^\pm (Lubarda et al., 1994). These operators are fourth-order tensors and are defined as:

$$\mathbb{P}_E^\pm = \frac{\partial \mathbf{E}^\pm}{\partial \mathbf{E}} = \frac{\partial}{\partial \mathbf{E}} (\langle E_\alpha \rangle^\pm \mathbf{n}_\alpha \otimes \mathbf{n}_\alpha) . \quad (22)$$

The second-order tensors $\mathbf{M}_\alpha := \mathbf{n}_\alpha \otimes \mathbf{n}_\alpha$ are defined as the eigenvalue bases related to the eigenvalue E_α . In the case of distinct eigenvalues $E_\alpha \neq E_\beta$, the classical results can be found in Miehe and Lambrecht (2001) and expressed as:

$$\frac{\partial E_\alpha}{\partial \mathbf{E}} = \mathbf{M}_\alpha, \quad \frac{\partial \mathbf{M}_\alpha}{\partial \mathbf{E}} = \sum_{\alpha \neq \beta}^2 \frac{1}{2(E_\alpha - E_\beta)} (\mathbb{G}_{\alpha\beta} + \mathbb{G}_{\beta\alpha}), \quad (23)$$

where the fourth-order tensor operator $\mathbb{G}_{\alpha\beta} = \hat{\mathbb{G}}(\mathbf{M}_\alpha, \mathbf{M}_\beta)$ with the coordinates representation is introduced as:

$$(\mathbb{G}_{\alpha\beta})_{\gamma\delta\varepsilon\zeta} := (\mathbf{M}_\alpha)_{\gamma\varepsilon} (\mathbf{M}_\beta)_{\delta\zeta} + (\mathbf{M}_\alpha)_{\gamma\zeta} (\mathbf{M}_\beta)_{\delta\varepsilon}. \quad (24)$$

With the notations as mentioned above and derivations, we can now explicitly express the projection tensors $\mathbb{P}_E^\pm = \partial \mathbf{E}^\pm / \partial \mathbf{E}$. The components of the projection tensors are given by:

$$\begin{aligned} \left(\frac{\partial \mathbf{E}^\pm}{\partial \mathbf{E}} \right)_{\gamma\delta\varepsilon\zeta} &= \frac{\partial (\mathbf{E}^\pm)_{\gamma\delta}}{\partial E_{\varepsilon\zeta}} \\ &= \frac{\partial}{\partial E_{\varepsilon\zeta}} (\langle E_\alpha \rangle^\pm (\mathbf{M}_\alpha)_{\gamma\delta}) \\ &= \frac{\partial \langle E_\alpha \rangle^\pm}{\partial E_{\varepsilon\zeta}} (\mathbf{M}_\alpha)_{\gamma\delta} + \langle E_\alpha \rangle^\pm \frac{\partial (\mathbf{M}_\alpha)_{\gamma\delta}}{\partial E_{\varepsilon\zeta}} \\ &= H(\pm E_\alpha) (\mathbf{M}_\alpha)_{\varepsilon\zeta} (\mathbf{M}_\alpha)_{\gamma\delta} + \\ &\quad \sum_{\alpha \neq \beta}^2 \frac{\langle E_\alpha \rangle^\pm}{2(E_\alpha - E_\beta)} \left((\mathbb{G}_{\alpha\beta})_{\gamma\delta\varepsilon\zeta} + (\mathbb{G}_{\beta\alpha})_{\gamma\delta\varepsilon\zeta} \right). \end{aligned} \quad (25)$$

Consequently, the positive and negative constitutive tensors \mathbb{C}^\pm can be obtained and reformulated as:

$$\begin{aligned} \mathbb{C}^\pm = & \left(\lambda - \frac{\lambda^2}{\lambda + 2\mu} \right) H(\pm \text{tr}(\mathbf{E})) \mathbb{J} + \\ & 2\mu \left(H(\pm E_\alpha) \mathbb{Q}_\alpha + \sum_{\alpha \neq \beta}^2 \frac{\langle E_\alpha \rangle^\pm}{2(E_\alpha - E_\beta)} (\mathbb{G}_{\alpha\beta} + \mathbb{G}_{\beta\alpha}) \right), \end{aligned} \quad (26)$$

with the fourth-order tensor $(\mathbb{Q}_\alpha)_{\gamma\delta\varepsilon\zeta} := (\mathbf{M}_\alpha)_{\varepsilon\zeta}(\mathbf{M}_\alpha)_{\gamma\delta}$. By replacing the constitutive tensor formulations within the internal stiffness matrix with the newly derived ones, the determination of the wrinkling states, as shown in Fig. 2, can be automated. In the case of a taut state, the constitutive tensor remains unchanged from its unmodified form. In the wrinkled state, the internal stiffness matrix primarily incorporates the positive part of the constitutive tensor, effectively minimizing compressive stresses. For slackening, a residual stiffness is introduced. This approach allows for the automatic identification and treatment of different wrinkling states, enabling improved convergence behavior in analyzing wrinkled membrane structures.

4. Discretization

In this section, we present the linearization of the Eq. (9) and discretization procedures for solving this equation. The presented discretization is suitable for any basis function, such as the Lagrange polynomial used in standard finite element analysis or Non-Uniform Rational B-Splines (NURBS) typically applied in isogeometric analysis (IGA), to name a few. IGA is a widely adopted technique in structural analysis due to its numerous advantages. To ensure conciseness, we refrain from reiterating these details here; more details can be found in the literature (Cottrell et al., 2009, Hughes et al., 2005).

In our research, we employ NURBS-based basis functions to discretize the displacement field. For a fundamental introduction to NURBS, we recommend referring to Piegl and Tiller (1996), Rogers (2001). The discretized displacement field is represented as follows:

$$\mathbf{u} = \sum_a^{n_{sh}} N^a \mathbf{u}^a, \quad (27)$$

where N^a denotes the shape functions, n_{sh} represents the total number of shape functions, and \mathbf{u}^a refers to the nodal displacement vectors with components u_i^a ($i = 1, 2, 3$) representing the global x -, y -, z -components. We establish an expression for the global degree of freedom number r of a nodal displacement, i.e., $r = 3(a - 1) + i$, such that $u_r = u_i^a$. In order to determine the variation of the displacement field with respect to u_r , the partial derivative of $\partial/\partial u_r$ is used:

$$\frac{\partial \mathbf{u}}{\partial u_r} = N^a \mathbf{e}_i, \quad (28)$$

where \mathbf{e}_i denote the global Cartesian base vectors. For more details, we refer to Kiendl et al. (2015). Subsequently, by deriving the variations of the internal virtual work δW^{int} and external virtual work δW^{ext} in the Eq. (9) with respect to u_r , the residual force vector \mathbf{R} is obtained and defined as:

$$R_r = F_r^{\text{int}} - F_r^{\text{ext}} = \int_A \mathbf{S} : \frac{\partial \mathbf{E}}{\partial u_r} t \, dA - \int_A \mathbf{f} \cdot \frac{\partial \mathbf{u}}{\partial u_r} \, dA, \quad (29)$$

where \mathbf{F}^{int} and \mathbf{F}^{ext} represent the vectors of the internal and external nodal loads, respectively. The linearization of Eq. (29) yields the tangential stiffness matrix \mathbf{K} , which comprises the internal stiffness matrix \mathbf{K}^{int} and external

stiffness matrix \mathbf{K}^{ext} , formulated as follows:

$$K_{rs} = K_{rs}^{\text{int}} - K_{rs}^{\text{ext}} = \int_A \frac{\partial \mathbf{S}}{\partial u_s} : \frac{\partial \mathbf{E}}{\partial u_r} + \mathbf{S} : \frac{\partial^2 \mathbf{E}}{\partial u_r \partial u_s} t \, dA - \int_A \frac{\partial \mathbf{f}}{\partial u_s} \cdot \frac{\partial \mathbf{u}}{\partial u_r} \, dA. \quad (30)$$

In order to solve the linearized equation system, the Newton-Raphson method is employed and given by:

$$\frac{\partial W}{\partial u_r} + \frac{\partial^2 W}{\partial u_r \partial u_s} \Delta u_s = 0, \quad (31)$$

where Δu_s denotes the components of the incremental displacements. Through the solution of the equation system, as mentioned earlier, we derive the incremental displacement vector $\Delta \mathbf{u}$, which ensures its accuracy subject to the precise computation of the residual vector \mathbf{R} , given by:

$$\mathbf{K} \Delta \mathbf{u} = -\mathbf{R}. \quad (32)$$

The Newton-Raphson method converges towards the desired solution by iteratively updating the displacement vector until the residual is minimized, leading to the accurate determination of the incremental displacement $\Delta \mathbf{u}$.

5. Numerical examples

In this section, we assess the capability of the proposed formulation in four numerical examples with analytical or reference solutions from the literature. All tests are conducted using nonlinear static isogeometric analysis, performed with NURBS. In order to show that our proposed formulation is applicable to standard finite element analysis, we also set the polynomial degree of the NURBS basis function as $p = 1$ for some cases because it is equivalent to first-order Lagrange polynomial when $p = 1$. The following

notations are used for various stresses presented in the results: $\boldsymbol{\sigma}$ indicates the Cauchy stress tensor, which is obtained by $\boldsymbol{\sigma} = (\det \mathbf{F})^{-1} \cdot \mathbf{F} \cdot \mathbf{S} \cdot \mathbf{F}^T$. Its first and second principal stresses are denoted as σ_1 and σ_2 , respectively. The residual norm applied in the analysis is defined with respect to the external forces magnitude as $\|\mathbf{R}\|/\|\mathbf{F}^{\text{ext}}\|$. The degradation factor $\eta = 10^{-4}$ is default for all numerical examples.

5.1. In-plane pure bending of a pre-tensioned rectangular membrane

The first numerical example considers a pre-stretched rectangular membrane under in-plane pure bending to evaluate the accuracy of our proposed model. Since an analytical solution was presented in Stein and Hedgepeth (1961), this example is considered a benchmark for studying partly wrinkled membranes. This problem has also been extensively investigated in the literature by various researchers as Ding et al. (2003), Jarasjarungkiat et al. (2009), Jeong and Kwak (1992), Liu et al. (2013), Lu et al. (2001), Miller et al. (1985), Wang et al. (2016). As depicted in Fig. 3, the membrane with

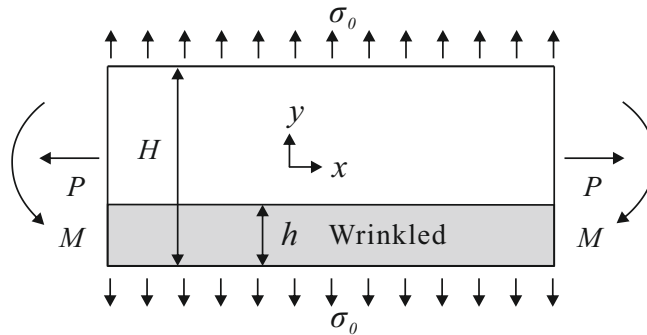


Figure 3: In-plane pure bending of a pre-tensioned rectangular membrane

the height H and the thickness t is subjected to a uniform stress σ_0 in the

y -direction, as well as a pair of the axial loads $P = \sigma_0 t H$ and the bending moments M at the lateral sides. By increasing the bending moments M , a band of vertical wrinkles of height h (highlighted in gray) appears along the bottom edge, and the band height h of the wrinkled zone is defined in Stein and Hedgepeth (1961) as:

$$\frac{h}{H} = \begin{cases} 0 & M/PH < 1/6 \\ 3M/PH - 1/2 & 1/6 \leq M/PH < 1/2 \end{cases}. \quad (33)$$

In the wrinkled region, the normal stress σ_x in the membrane is eliminated, whereas, in other regions, it is linearly distributed along the height H . The normal stress distribution can be calculated using the following expression:

$$\frac{\sigma_x}{\sigma_0} = \begin{cases} \frac{2(y/H - h/H)}{(1 - h/H)^2} & h/H < y/H \leq 1 \\ 0 & 0 \leq y/H \leq h/H \end{cases}. \quad (34)$$

The simulation setup for this problem is presented in Fig. 4, where we use

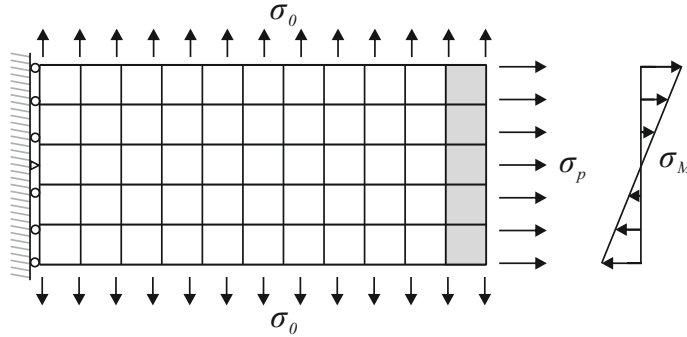


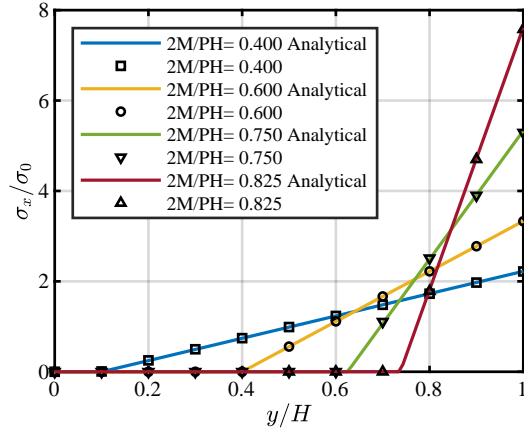
Figure 4: Numerical simulation setting for the right half of the rectangular membrane under in-plane bending

55 (11×5) bi-quadratic isogeometric membrane elements to solve the problem, following the recommendation in Nakashino and Natori (2005). Only

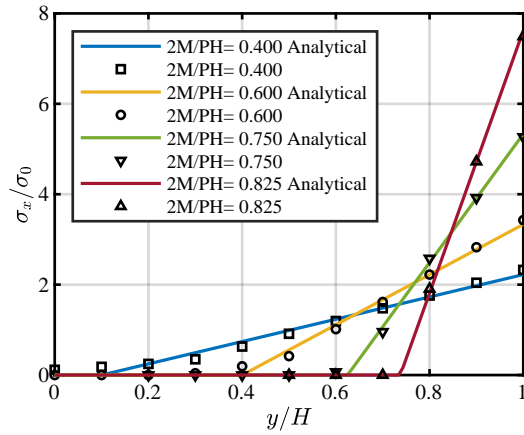
the right half of the membrane is modeled due to its symmetry, and the displacements in the x -direction on the left are constrained. The middle point of the left edge is also prevented from deforming in the y -direction. As illustrated, the axial load P and bending moment M are replaced by equivalent stresses $\sigma_p = P/tH$ and $\sigma_M = 6M/tH^2(2y/H - 1)$, respectively. In order to withstand compressive stresses and maintain a uniform rotation, the five elements on the right are assumed to remain taut. Thus, these elements are modeled as the standard membrane elements without embedding the wrinkling model.

First, we test the new wrinkling model in this example with different Poisson's ratios. Fig. 5 shows the normal stress σ_x distribution with respect to the applied stress σ_0 along the height H . Here, we use y/H -ratio, i.e., the stress-measured position y related to the height H , as x -axis to unify the results. Different curves exhibit the results for different values of the bending moment-force ratio ($2M/PH$). For the case of Poisson's ratio $\nu = 0$, the wrinkling model accurately predicts the results, as shown in Fig. 5(a), with excellent agreement to the analytical solutions. However, a slight difference is observed for the case of $\nu = 0.3$, as shown in Fig. 5(b). This deviation is caused by the fact, as mentioned in Section 3, that our wrinkling model is strain-based. Thus, the second principal stress σ_2 evaluated by our model is not always equal to zero. In contrast, the wrinkling criterion used in the analytical solution is based on principal stresses. Thereby, the analytically computed stresses are enforced to satisfy the uniaxial tension condition. Although the Poisson effect could influence the stress response predicted by the proposed model compared to the analytical solutions, the difference observed

in our model can be neglected in practical applications, as demonstrated by the following numerical examples.



(a) Poisson's ratio $\nu = 0$

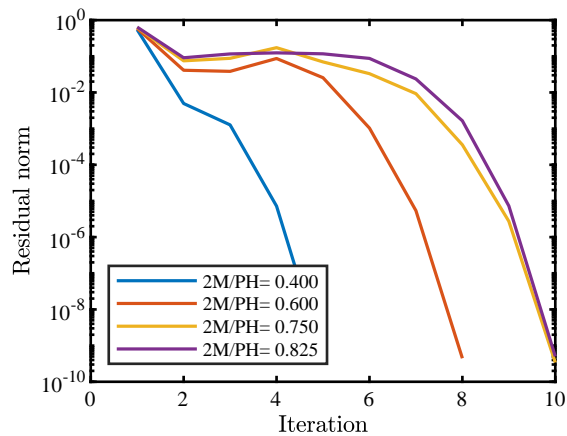


(b) Poisson's ratio $\nu = 0.3$

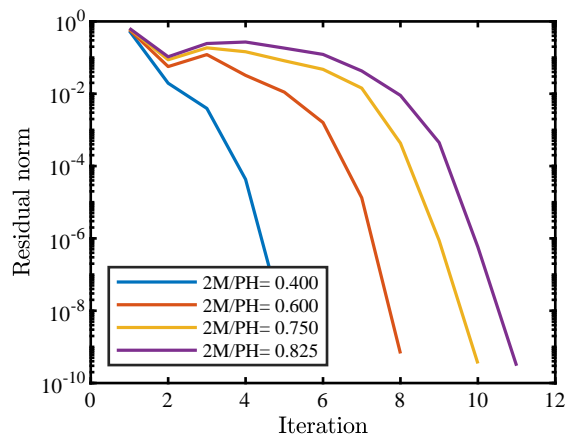
Figure 5: Normal stress σ_x distribution along the height H with the newly proposed wrinkling model

In addition, in order to show the convergence behavior of the proposed

model, we plot the number of iterations during the second load step in Fig. 6, where we can find the most iterations in it compared to the other load steps.



(a) Poisson's ratio $\nu = 0$



(b) Poisson's ratio $\nu = 0.3$

Figure 6: Convergence behavior of rectangular membrane under in-plane bending during the second load step

From Figs. 6(a) and 6(b), it can be seen that the new model can achieve

a good convergence and increasing bending moment requires more iterations to reach the preset tolerance 10^{-8} .

To prove the robustness of the proposed wrinkling model during mesh refinement, we conduct a mesh convergence study by plotting the normal stresses σ_x along with the height H under various mesh sizes with a Poisson's ratio $\nu = 0$ in Fig. 7. The results of the mesh convergence studies confirm that the accuracy and robustness of the proposed model are not affected by changes in the element size. In Appendix A, the results for $p = 1$, $\nu = 0$, $\eta = 10^{-4}$ are attached in Fig. A.22 to evidence that the newly proposed model can be equally applied to standard finite element analysis.

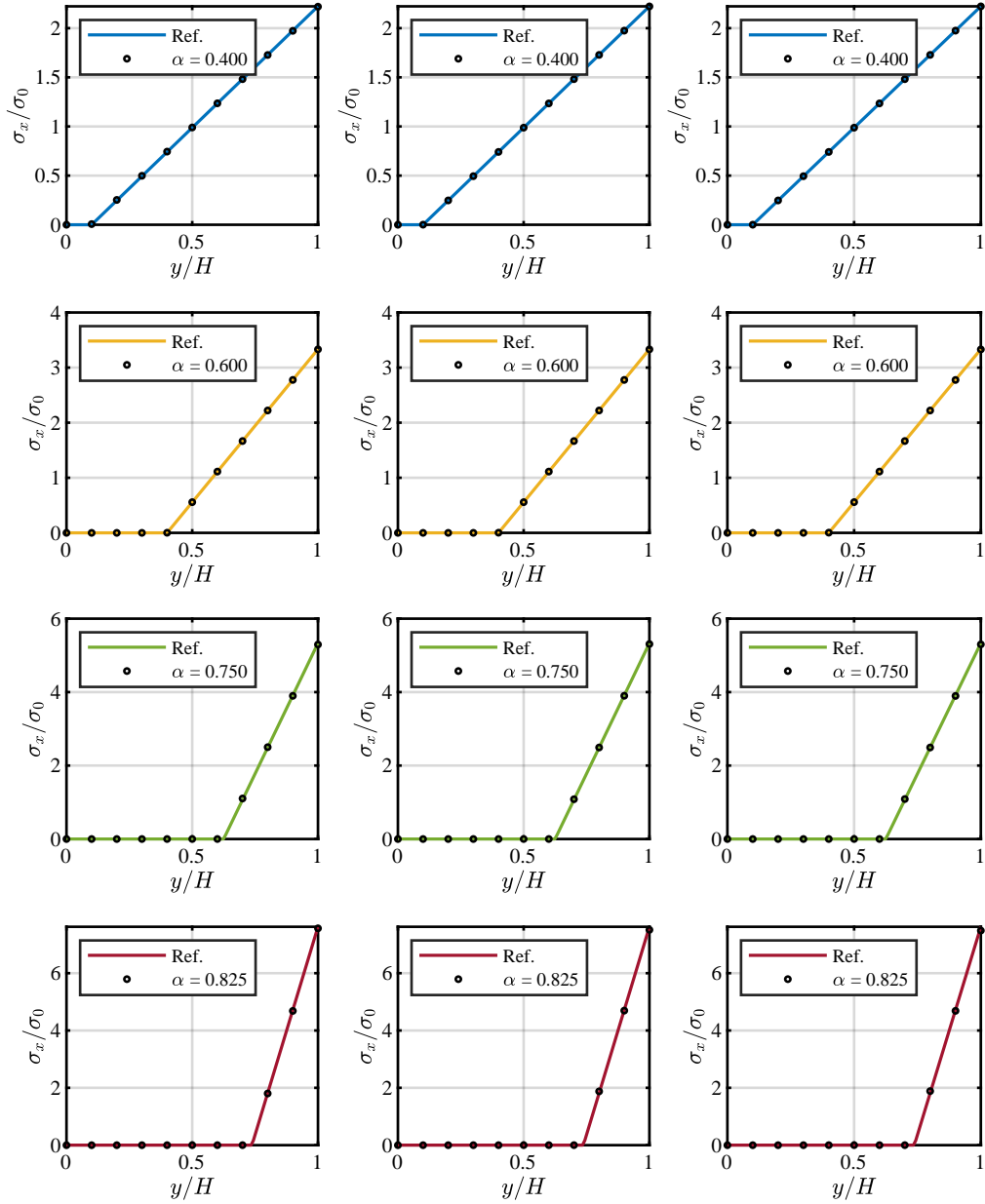


Figure 7: Normal stress σ_x distribution along the height H computed by the proposed model with Poisson's ratio $\nu = 0$, degradation factor $\eta = 10^{-4}$, polynomial degree $p = 2$, and $\alpha = 2M/PH$. In the left, middle, and right columns, mesh refinement is carried out as 11×5 , 23×11 , and 43×21 , respectively.

5.2. Flat square membrane under corner loads

As a second example, we present a verification of the proposed wrinkling model using the case of a square membrane subjected to corner loads of T_1 and T_2 with nonzero Poisson's ratio, which is discussed in Jarasjarungkiat et al. (2009), Wang et al. (2014), Wong and Pellegrino (2006a,c). The mem-

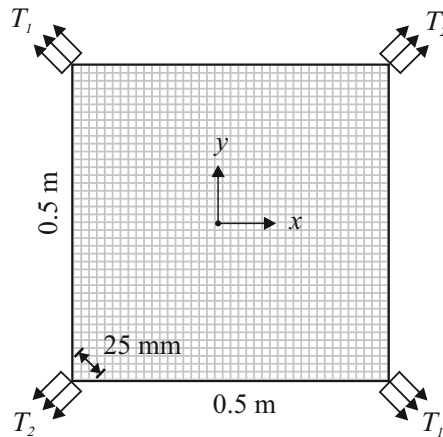


Figure 8: Flat square membrane under corner loads T_1 and T_2

brane possesses a length of 0.5 m and a thickness of 25 μm . It undergoes the diagonal pairs of equal and opposite forces T_1 and T_2 at the four corners, as shown in Fig. 8. As suggested in Jarasjarungkiat et al. (2009), the central point of the membrane is fixed to prevent rigid body motions. In addition, the movement in x -direction of the middle point at the top edge is also constrained to avoid rotation. We perform numerical analyses for the various values of the T_1/T_2 -ratio, where T_1 is increased from 5 N to 20 N, while T_2 is kept constant at 5 N for all cases.

The material parameters used in this study are Young's modulus $E = 3500$ MPa and Poisson's ratio $\nu = 0.31$. The square membrane is discretized

using 40×40 cubic elements. We plot the first principal stress distributions σ_1 under various load ratios T_1/T_2 in Figs. 9(a)-(d). The new model appears

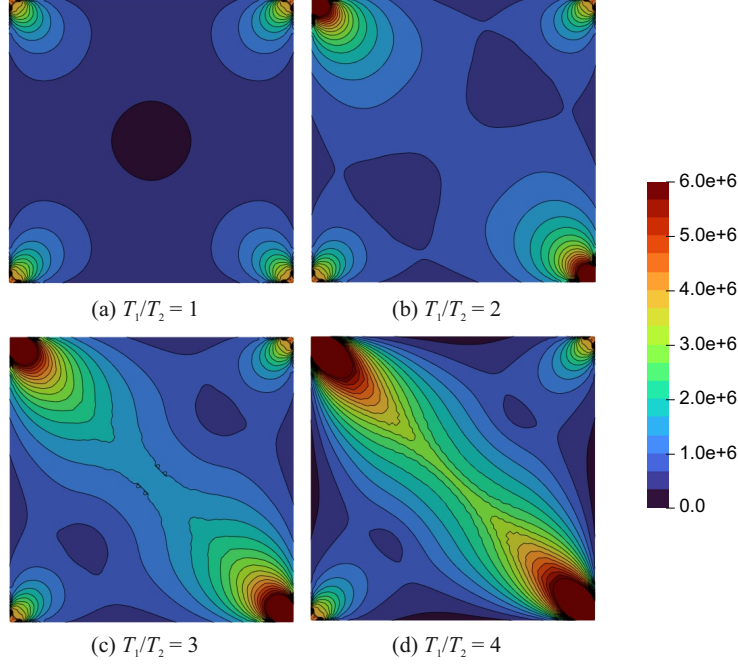


Figure 9: Contours of the first principal stresses σ_1 (Pa) under the different values of the T_1/T_2 -ratio

to attain the comparable first principal stress distribution patterns under various load ratios T_1/T_2 compared to the thin shell solutions (Wong and Pellegrino, 2006c) and those predicted by tension field theory-based wrinkling models (Jarasjarungkiat et al., 2009, Wang et al., 2014). Additionally, we plot the wrinkling intensity under the different values of the T_1/T_2 ratio in Fig. 10. The wrinkling intensity shows the absolute values of the negative second eigenvalues of the strain tensor multiplied with the norm of the first eigenvector if the wrinkling state is wrinkled. Otherwise, in the case of

taut or slackened states, the value would be zero. In Fig. 11, the wrinkling

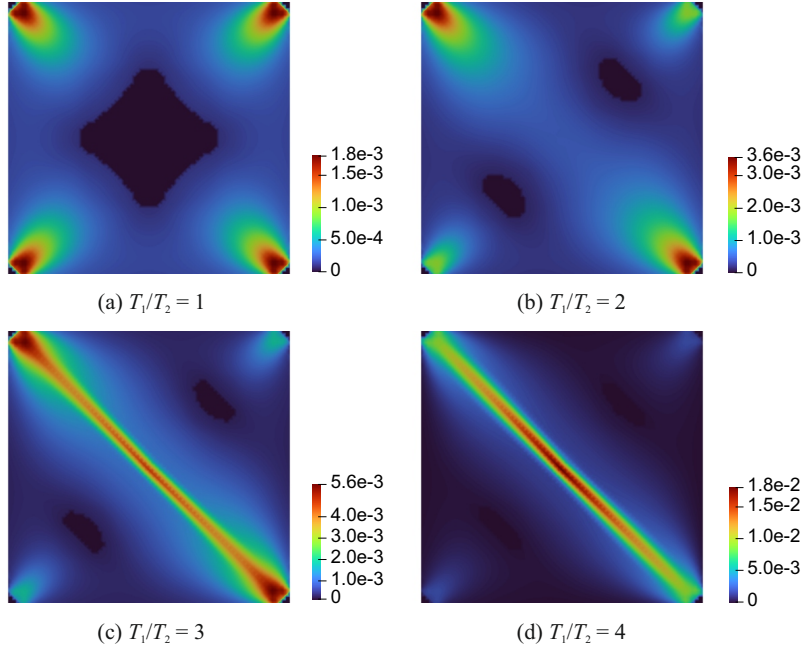


Figure 10: Wrinkling intensity under the different values of the T_1/T_2 -ratio

trajectories are presented. The regions marked by lines indicate the wrinkled zones, the lines show the direction of the first eigenvector of the strains, and the line length is scaled according to the corresponding second eigenvalues. The areas without lines are the taut or slackened regions. As shown in Fig. 11, it can be recognized that the wrinkles are mainly concentrated in the diagonal by increasing the load ratio, similar to the fact observed in the experiments (Wong and Pellegrino, 2006a) and the numerical results (Jarasjarunkiat et al., 2009, Wang et al., 2014, Wong and Pellegrino, 2006c).

Fig. 12 presents a graphical representation illustrating the convergence performance of the square membrane subjected to various corner load ratios. The convergence performance is measured by tracking the number of

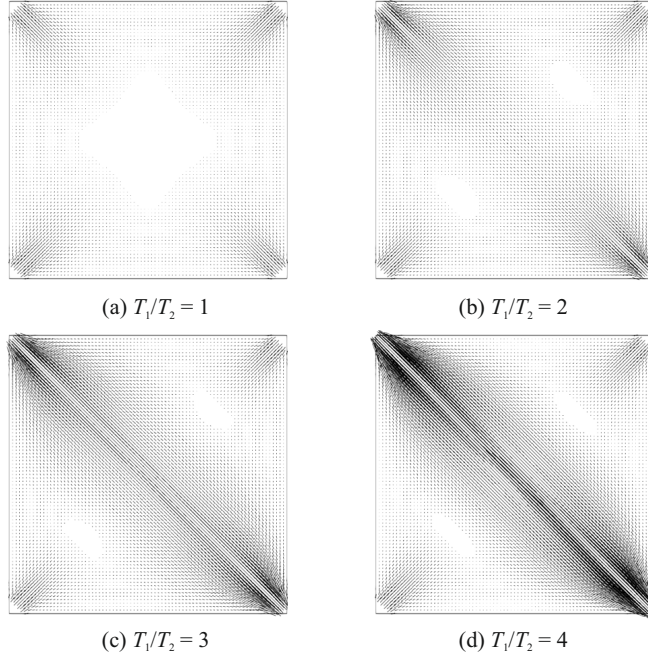
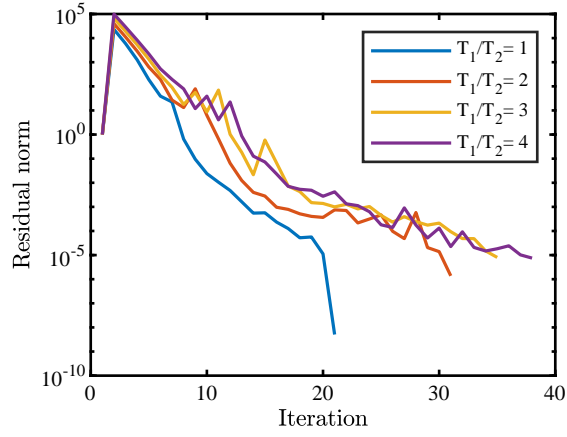
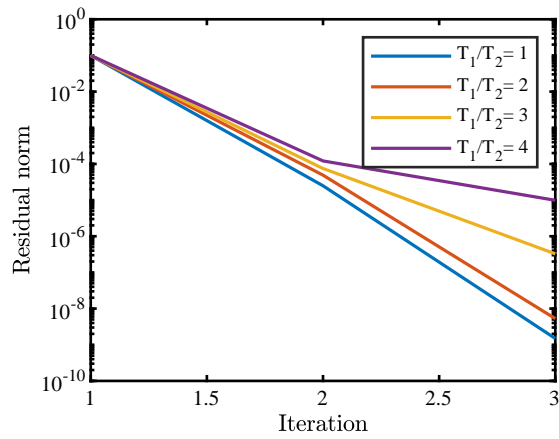


Figure 11: Wrinkling trajectories under the different values of the T_1/T_2 -ratio

iterations required in the first and last load steps. Throughout this investigation, a specific residual criterion of 10^{-5} is established to evaluate the convergence of the numerical solution. As depicted in Fig. 12(a), in the case of ratio $T_1/T_2 = 1$, it requires fewer iterations to reach the tolerance compared to other cases because the diagonal wrinkles that can deteriorate the convergence behavior have not formed yet in the case of $T_1/T_2 = 1$. The convergence behavior from the second load step follows a similar pattern to the last load step. Hence, we show the iterations in the last load step as illustrated in Fig. 12(b).



(a) Residual norm in the first step



(b) Residual norm in the last step

Figure 12: Convergence behavior of the square membrane under corner loads with various T_1/T_2 -ratios

5.3. Inflation of a square isotropic airbag

In the third example, we model the inflation of a square airbag, which is a commonly used benchmark for validating finite element-based wrinkling algorithms; related works are referred to Contri and Schrefler (1988), Diaby et al. (2006), Gil and Bonet (2007), Jarasjarungkiat et al. (2008, 2009), Kang and Im (1999), Le Meitour et al. (2021b), Lee and Youn (2006). The initially

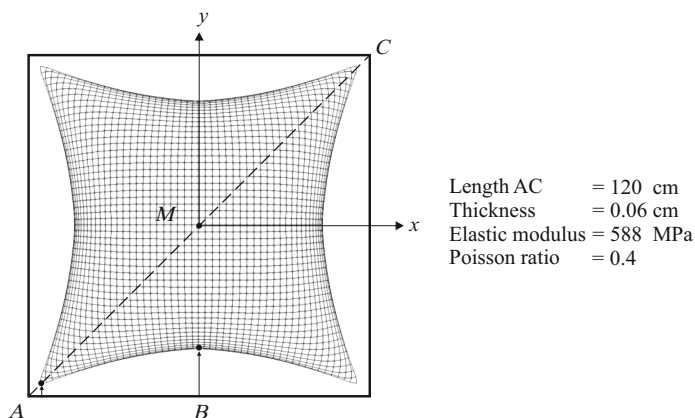


Figure 13: Airbag simulation setup

flat square airbag has a diagonal length of $AC = 120$ cm and a thickness of $t = 0.06$ cm, as Fig. 13 shows. It is loaded by a displacement-dependent pressure P perpendicular to the surface, increasing to 5000 Pa gradually. We did not consider the external stiffness matrix produced by pressure in our element formulation for simplification. Due to the symmetry, only a quarter of the airbag is simulated. Thus, the symmetric boundary conditions are applied to the inner edges, while the movements of outer edges in the z -direction are constrained. The material of the airbag is assumed to be linear isotropic, with an elastic modulus $E = 588$ MPa and Poisson's ratio $\nu = 0.4$.

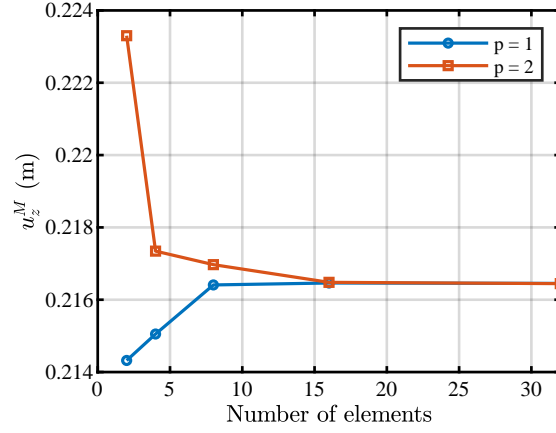
As indicated in Diaby et al. (2006), the inflation of a square airbag poses a specific difficulty caused by the high singularity of the stiffness matrix at the initial stage due to the normal pressure applied to the membrane surface. One possibility is to use dynamic relaxation (DR) (Nakashino et al., 2020) to overcome this numerical obstacle. DR approximates a static equilibrium solution through a pseudo-dynamic transient analysis. However, a more straightforward alternative is to stretch the membrane along the x - and y -directions with dead forces on the two outer edges, as suggested in Diaby et al. (2006), Lee and Youn (2006). These forces are gradually reduced and removed when the pressure P reaches a fixed value. This approach enables us to avoid the initial singularity issue and obtain an accurate solution for the airbag inflation simulation.

A comprehensive comparison between the results from the existing literature and the present work is presented in Tab. 1. It compares the vertical

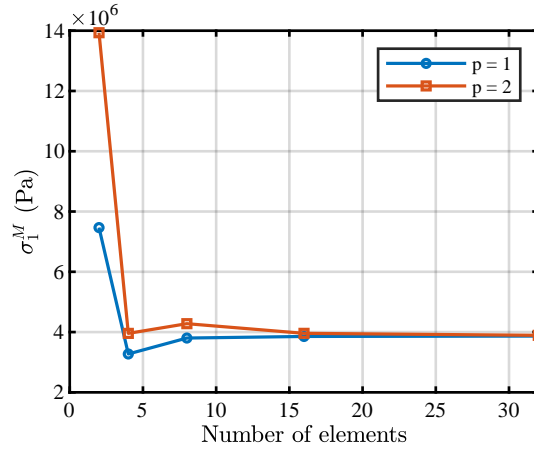
Table 1: Comparison of airbag results from literature and present work

	Contri and Schrefler (1988)	Kang and Im (1999)	Diaby et al. (2006)	Jarasjarungkiat et al. (2009)	Present work $p = 1$	Present work $p = 2$
u_z^M (m)	0.217	0.214	0.2245	0.2175	0.2165	0.2164
u_y^A (m)	0.045	0.041	0.0307	0.0349	0.0362	0.0351
u_y^B (m)	0.110	0.119	0.1158	0.1203	0.1210	0.1212
σ_1^M (MPa)	3.5	–	–	3.9	3.9	3.9

displacement u_z^M at point M and the displacements of the y -components at points A and B , denoted as u_y^A and u_y^B , respectively. Moreover, the first principal stress σ_1^M at point M was also measured in some of the references. By comparing our computed results with the outcomes reported in previous studies, a substantial agreement is observed, particularly concerning the prediction of the vertical displacements u_z^M and the first principal stresses σ_1^M . It indicates that the slight difference due to the Poisson effect shown in



(a)



(b)

Figure 14: Convergence study of the vertical displacement (a) and the first principal stress (b) at point M during mesh refinement

the first benchmark can be neglected in complicated examples. In order to demonstrate the mesh independence of the proposed wrinkling formulation, we focus on analyzing the vertical displacements at point M and the first

principal stresses at the same location while progressively refining the mesh using linear ($p = 1$) and quadratic ($p = 2$) membrane elements. The results are presented in Fig. 14(a) for the vertical displacements and in Fig. 14(b) for the first principal stresses.

We plot the distributions of the first and second principal stresses $\sigma_{1/2}$ within the inflated airbag shown in Fig. 15. The maximum values of the

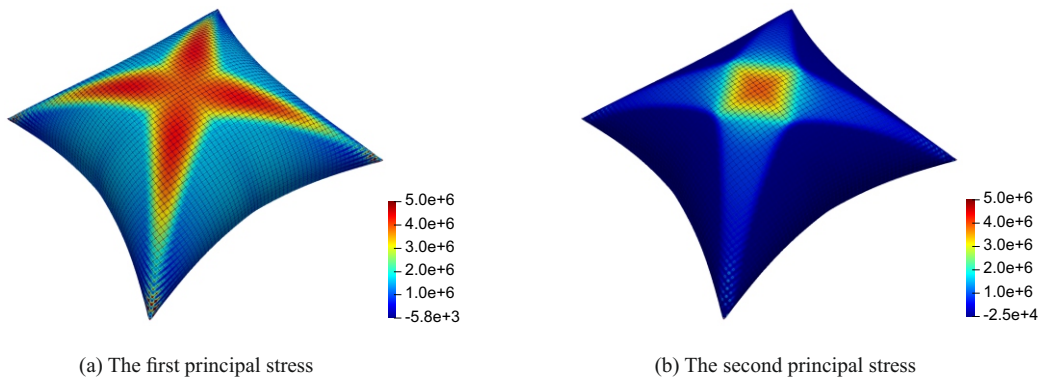


Figure 15: Contours of the first and second principal stresses $\sigma_{1/2}$ (Pa) distributed in the inflated airbag

first and second principal stresses are approximately $\sigma_1 = 49$ MPa and $\sigma_2 = 17$ MPa, both occurring at the corners. However, due to the excessive magnitude of these values, the stress distribution diagram lacks clarity. Therefore, in the stress contour plot, we present a more reasonable and scaled representation. Besides, These principal stress distributions align with the observed wrinkle trajectories illustrated in Fig. 16. Precisely, the regions in proximity to the midpoint of the edges of the airbag exhibit pronounced wrinkling phenomena, while the central regions remain taut and devoid of wrinkles.

Fig. 17 showcases the convergence behavior of the airbag during the final load step under different mesh sizes. The plot reveals a noteworthy trend

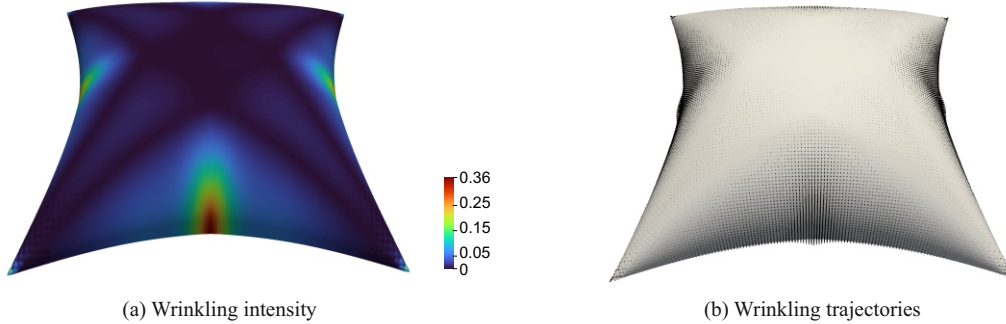
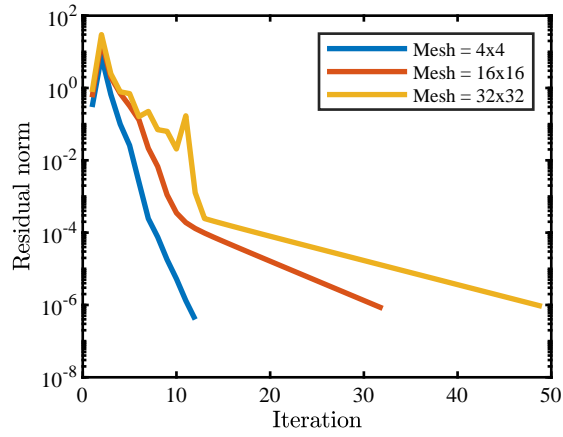
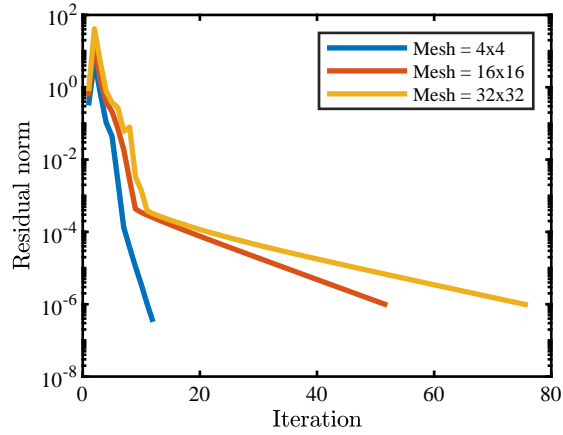


Figure 16: Illustration of the wrinkled zone in a fully inflated square airbag

wherein the mesh refinement leads to increased iterations required to attain the predetermined residual criterion 10^{-6} . Furthermore, when the polynomial order is elevated, more iterations are necessary. In addition, we also investigate the impact of the degradation factor η on the airbag deformation. The displacement u_z^M and u_y^B converge to different values if the degradation factor is very small, such as $\eta = 10^{-8}$. This discrepancy arises because there is almost no resistance against the compression at the right edge, causing elements along this edge to interpenetrate, a phenomenon analogous to observations in a prior study (Nakashino et al., 2020). This unphysical behavior can be effectively avoided with an appropriate degradation factor η . In the case of $\eta = 0$, it could influence converge behavior when slackening occurs, without taking residual stiffness into account. Therefore, we set $\eta = 10^{-4}$ as a proper value to mitigate these issues and ensure convergence, striking a balance between avoiding excessive degradation and preventing unrealistic behavior in the simulation.



(a) Residual norm of the last step with $p = 1$



(b) Residual norm of the last step with $p = 2$

Figure 17: Convergence behavior of airbag during the last step with different mesh

5.4. Hanging blanket under self-weight

While all the benchmark examples above represent prestretched membranes, in this final example, we consider a “loose” membrane loaded by self-weight only. It represents a hanging blanket supported at its corners, as shown in Fig. 18. All four corners are supported rigidly in z -direction, while elastic supports are applied in the x - y -plane as shown in Fig. 18 such that the blanket can undergo large deformations due to self-weight. The length of the

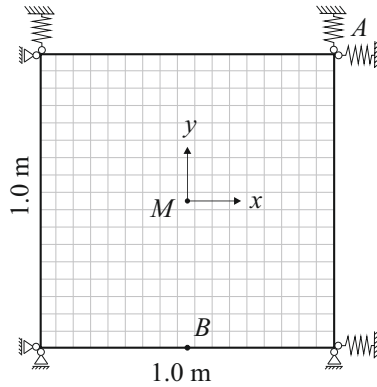


Figure 18: Hanging blanket under self-weight

blanket is $L = 1$ m and its thickness $t = 1.177$ mm. The material parameters applied in this example are Young’s modulus $E = 30\,000$ Pa, surface density $\rho = 0.144$ kg m⁻² for self-weight. Poisson’s ratio varies between $\nu = 0$ and $\nu = 0.3$, and the elastic supports are applied via the penalty formulation presented in Herrema et al. (2019), with a penalty parameter $\alpha = 10^{-2}$. A mesh of 25×25 bi-quadratic elements is used to model the wrinkling behavior of the square hanging blanket.

Fig. 19 depicts the deformation and the first and second principal stresses. In Fig. 20, the wrinkling intensity and trajectories are plotted. As can be

seen, significant wrinkling phenomena are prominently observed in the regions near the four corners and four edges of the blanket. In contrast, the central regions remain taut without any wrinkles. For validation, we also perform simulations with the wrinkling model proposed in Nakashino and Natori (2005) using the same setup and mesh, and its results are remarked as a reference.

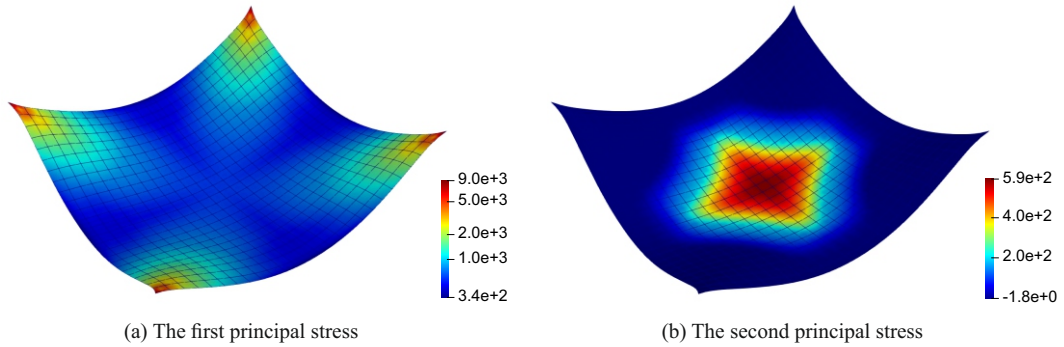


Figure 19: Distribution of the first and second principal stresses $\sigma_{1/2}$ (Pa) with $\nu = 0.3$

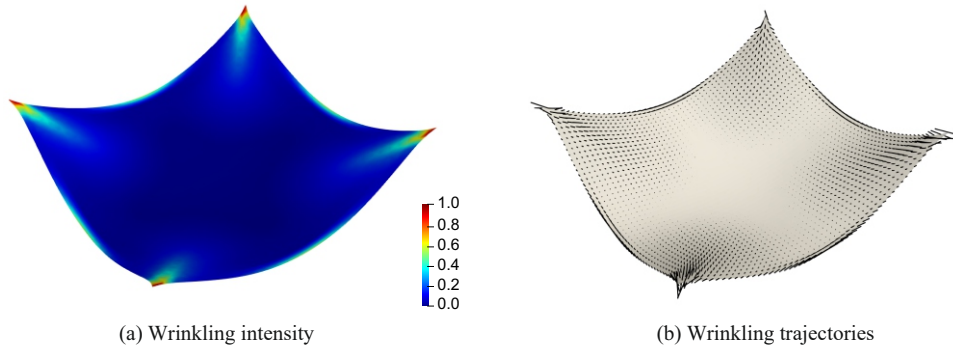


Figure 20: Illustration of the wrinkled zone in a hanging blanket with $\nu = 0.3$

Tab. 2 demonstrates very good agreement between the newly proposed model and the reference in predicting the displacements at points A , B , and

M , denoted as u_x^A , u_x^B and u_z^M , respectively, as well as the first principal stress σ_1^M at the middle point M when considering a Poisson’s ratio $\nu = 0$. The

Table 2: Comparison of the displacements and first principal stress with $\nu = 0$

Mesh (25x25)	u_z^M (m)	u_x^A (m)	u_x^B (m)	σ_1^M (MPa)
Reference	-0.2895	-0.03661	-0.01830	637.68
New model	-0.2898	-0.03671	-0.01836	611.11

results in Tab. 3 exhibit distinguishable variations between the two models for a nonzero Poisson’s ratio. This discrepancy arises since the new wrinkling model is strain-based, while the wrinkling criterion used in the reference is mixed. Besides, the reference model can satisfy the uniaxial tension condition consistently. However, the discrepancies remain within an acceptable range, indicating that the proposed model still provides reasonable predictions even for cases where the uniaxial tension condition is not strictly met.

Table 3: Comparison of the displacements and first principal stress with $\nu = 0.3$

Mesh (25x25)	u_z^M (m)	u_x^A (m)	u_x^B (m)	σ_1^M (MPa)
Reference	-0.2833	-0.03406	-0.01703	642.66
New model	-0.2956	-0.03290	-0.01645	586.14

The convergence performances of the two models are compared across various Poisson’s ratios in Fig. 21. The results indicate that the new model exhibits significantly superior convergence compared to the reference. Specifically, the new wrinkling model achieves convergence within approximately ten iterations, whereas the reference requires over one hundred iterations, particularly when the Poisson’s ratio is zero. That attributes the advantages of the new model, which is consistently derived from the strain energy density. These findings underscore the improved convergence behavior of the

proposed model, and the substantial reduction in the number of iterations needed for convergence demonstrates the advantages and practicality of the proposed model in simulating and analyzing wrinkling behavior in membrane structures.

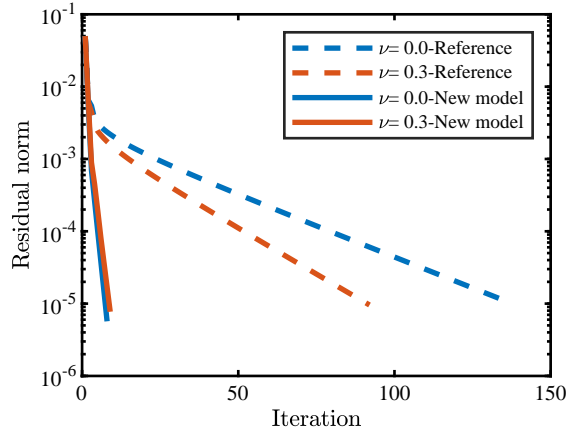


Figure 21: Comparison of the convergence behavior of two models during the last step with various Poisson's ratios

6. Conclusion

We have presented a variationally consistent membrane wrinkling model based on the spectral decomposition of the strain tensor, which can perform well in wrinkled membrane analysis and improve convergence issues caused by the wrinkling phenomenon. In this wrinkling model, we decompose the strain tensor into positive and negative components based on the eigenvalues. It allows us to split the strain energy density into positive and negative parts. We reduce the negative strain energy density arising from the negative component of the strain tensor by introducing a degradation factor, enabling us to minimize the compressive stresses. Furthermore, we consistently derive

the modified strain energy density with respect to strain variables to determine new stress tensor and constitutive tensor formulations. In addition, the eigenvector directions are considered to track the wrinkling directions in the new membrane wrinkling model.

To assess the effectiveness of the proposed method, we conducted a series of tests on analytical, numerical and experimental benchmarks for membrane wrinkling problems. We have employed this model in standard finite element and isogeometric analysis formulations, showing its generality. The results of these tests indicate that the newly proposed wrinkling model performs well in accurately predicting the mechanical responses of wrinkled thin membranes and shows a very good convergence behavior.

One possible direction for future research on the proposed approach is its extension to hyperelastic material models since the current model presented in this study is limited to isotropic linear elasticity. Another future research direction is the simultaneous spectral decomposition of the strain and stress tensors into positive and negative components. Thus, the wrinkling criterion would rely no longer solely on strain but on a widely used mixed stress-strain criterion.

Appendix A.

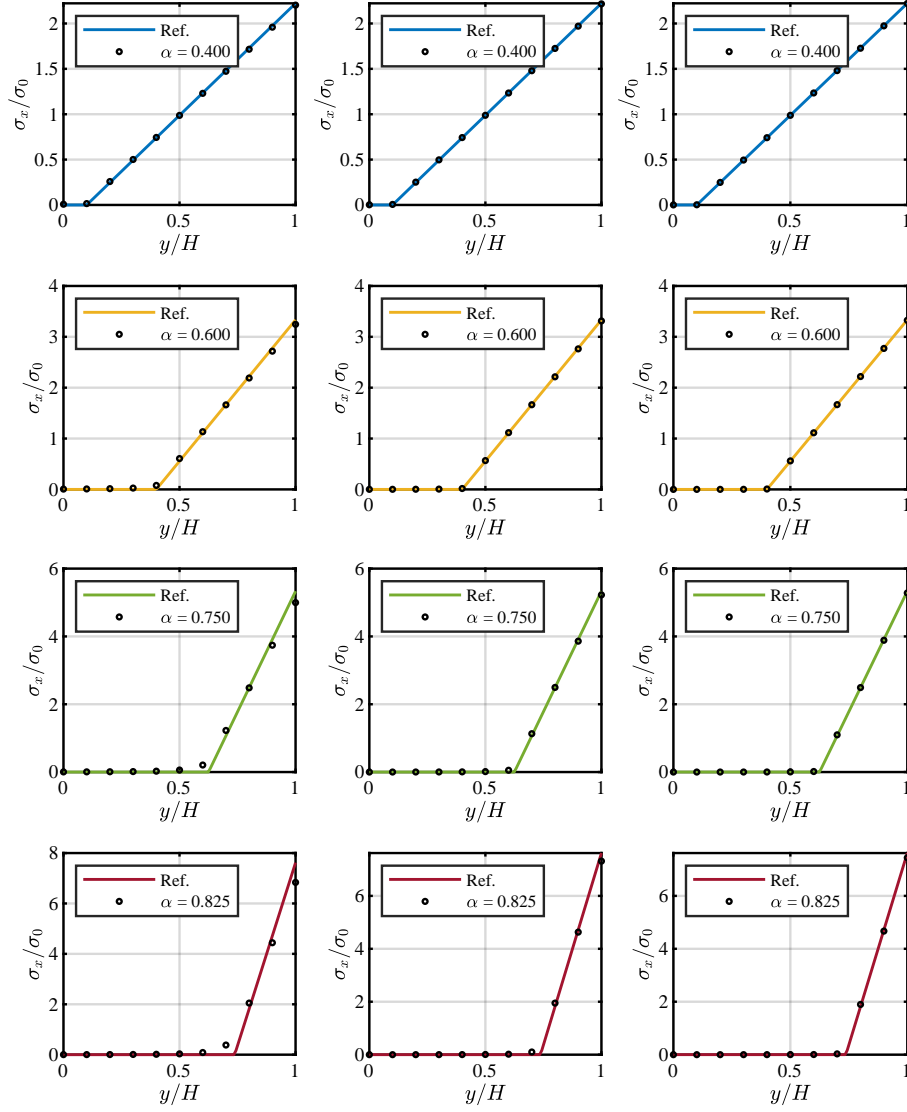


Figure A.22: Normal stress σ_x distribution along the height H computed by the proposed model with Poisson's ratio $\nu = 0$, degradation factor $\eta = 10^{-4}$, polynomial degree $p = 1$, and $\alpha = 2M/PH$. In the left, middle, and right columns, mesh refinement is carried out as 11×5 , 23×11 , and 43×21 , respectively.

References

- T. Akita, K. Nakashino, M. Natori, and K. Park. A simple computer implementation of membrane wrinkle behaviour via a projection technique. *International journal for numerical methods in engineering*, 71(10):1231–1259, 2007.
- E. Cerda and L. Mahadevan. Geometry and physics of wrinkling. *Physical review letters*, 90(7):074302, 2003.
- P. Contri and B. Schrefler. A geometrically nonlinear finite element analysis of wrinkled membrane surfaces by a no-compression material model. *Communications in applied numerical methods*, 4(1):5–15, 1988.
- J. A. Cottrell, T. J. Hughes, and Y. Bazilevs. *Isogeometric analysis: toward integration of CAD and FEA*. John Wiley & Sons, 2009.
- A. Diaby, C. Wielgosz, et al. Buckling and wrinkling of prestressed membranes. *Finite elements in Analysis and Design*, 42(11):992–1001, 2006.
- H. Ding, B. Yang, M. Lou, and H. Fang. New numerical method for two-dimensional partially wrinkled membranes. *AIAA journal*, 41(1):125–132, 2003.
- M. Epstein and M. A. Forcinito. Anisotropic membrane wrinkling: theory and analysis. *International Journal of Solids and Structures*, 38(30-31):5253–5272, 2001.
- F. G. Flores and E. Oñate. Wrinkling and folding analysis of elastic mem-

- branes using an enhanced rotation-free thin shell triangular element. *Finite Elements in Analysis and Design*, 47(9):982–990, 2011.
- C. Fu, H.-H. Dai, and F. Xu. Computing wrinkling and restabilization of stretched sheets based on a consistent finite-strain plate theory. *Computer Methods in Applied Mechanics and Engineering*, 384:113986, 2021.
- A. J. Gil and J. Bonet. Finite element analysis of partly wrinkled reinforced prestressed membranes. *Computational Mechanics*, 40:595–615, 2007.
- E. Haseganu and D. Steigmann. Analysis of partly wrinkled membranes by the method of dynamic relaxation. *Computational Mechanics*, 14(6):596–614, 1994.
- A. J. Herrema, E. L. Johnson, D. Proserpio, M. C. Wu, J. Kiendl, and M.-C. Hsu. Penalty coupling of non-matching isogeometric kirchhoff–love shell patches with application to composite wind turbine blades. *Computer Methods in Applied Mechanics and Engineering*, 346:810–840, 2019.
- J. Hornig and H. Schoop. Closed form analysis of wrinkled membranes with linear stress–strain relation. *Computational mechanics*, 30(4):259–264, 2003.
- T. J. Hughes, J. A. Cottrell, and Y. Bazilevs. Isogeometric analysis: Cad, finite elements, nurbs, exact geometry and mesh refinement. *Computer methods in applied mechanics and engineering*, 194(39-41):4135–4195, 2005.
- T. Iwasa, M. Natori, and K. Higuchi. Evaluation of tension field theory for

- wrinkling analysis with respect to the post-buckling study. *J. Appl. Mech.*, 71(4):532–540, 2004.
- A. Jarasjarungkiat, R. Wüchner, and K.-U. Bletzinger. A wrinkling model based on material modification for isotropic and orthotropic membranes. *Computer methods in applied mechanics and engineering*, 197(6-8):773–788, 2008.
- A. Jarasjarungkiat, R. Wüchner, and K.-U. Bletzinger. Efficient sub-grid scale modeling of membrane wrinkling by a projection method. *Computer Methods in Applied Mechanics and Engineering*, 198(9-12):1097–1116, 2009.
- D. G. Jeong and B. M. Kwak. Complementarity problem formulation for the wrinkled membrane and numerical implementation. *Finite elements in analysis and design*, 12(2):91–104, 1992.
- S. Kang and S. Im. Finite element analysis of wrinkling membranes. *Journal of Applied Mechanics*, 64(2):263–269, 06 1997.
- S. Kang and S. Im. Finite element analysis of dynamic response of wrinkling membranes. *Computer Methods in Applied Mechanics and Engineering*, 173(1-2):227–240, 1999.
- J. Kiendl, M.-C. Hsu, M. C. Wu, and A. Reali. Isogeometric kirchhoff–love shell formulations for general hyperelastic materials. *Computer Methods in Applied Mechanics and Engineering*, 291:280–303, 2015.
- J. Kiendl, M. Ambati, L. De Lorenzis, H. Gomez, and A. Reali. Phase-field

- description of brittle fracture in plates and shells. *Computer Methods in Applied Mechanics and Engineering*, 312:374–394, 2016.
- H. Le Meitour, G. Rio, H. Laurent, A. Lectez, and P. Guigue. Analysis of wrinkled membrane structures using a plane stress projection procedure and the dynamic relaxation method. *International Journal of Solids and Structures*, 208:194–213, 2021a.
- H. Le Meitour, G. Rio, H. Laurent, A. Lectez, and P. Guigue. Analysis of wrinkled membrane structures using a plane stress projection procedure and the dynamic relaxation method. *International Journal of Solids and Structures*, 208:194–213, 2021b.
- E.-S. Lee and S.-K. Youn. Finite element analysis of wrinkling membrane structures with large deformations. *Finite Elements in Analysis and Design*, 42(8-9):780–791, 2006.
- C. Liu, Q. Tian, D. Yan, and H. Hu. Dynamic analysis of membrane systems undergoing overall motions, large deformations and wrinkles via thin shell elements of ancf. *Computer Methods in Applied Mechanics and Engineering*, 258:81–95, 2013.
- X. Liu, C. H. Jenkins, and W. W. Schur. Large deflection analysis of pneumatic envelopes using a penalty parameter modified material model. *Finite Elements in Analysis and Design*, 37(3):233–251, 2001.
- K. Lu, M. Accorsi, and J. Leonard. Finite element analysis of membrane wrinkling. *International Journal for numerical methods in engineering*, 50(5):1017–1038, 2001.

- V. Lubarda, D. Krajcinovic, and S. Mastilovic. Damage model for brittle elastic solids with unequal tensile and compressive strengths. *Engineering Fracture Mechanics*, 49(5):681–697, 1994.
- E. Mansfield. Tension field theory, a new approach which shows its duality with inextensional theory. In *Applied Mechanics: Proceedings of the Twelfth International Congress of Applied Mechanics, Stanford University, August 26–31, 1968*, pages 305–320. Springer, 1969.
- C. Miehe and M. Lambrecht. Algorithms for computation of stresses and elasticity moduli in terms of seth–hill’s family of generalized strain tensors. *Communications in numerical methods in engineering*, 17(5):337–353, 2001.
- C. Miehe, M. Hofacker, and F. Welschinger. A phase field model for rate-independent crack propagation: Robust algorithmic implementation based on operator splits. *Computer Methods in Applied Mechanics and Engineering*, 199(45-48):2765–2778, 2010.
- R. K. Miller and J. M. Hedgepeth. An algorithm for finite element analysis of partly wrinkled membranes. *AIAA journal*, 20(12):1761–1763, 1982.
- R. K. Miller, J. M. Hedgepeth, V. I. Weingarten, P. Das, and S. Kahyai. Finite element analysis of partly wrinkled membranes. In *Advances and Trends in Structures and Dynamics*, pages 631–639. Elsevier, 1985.
- Y. Miyazaki. Wrinkle/slack model and finite element dynamics of membrane. *International Journal for Numerical Methods in Engineering*, 66(7):1179–1209, 2006.

- J. Mosler. A novel variational algorithmic formulation for wrinkling at finite strains based on energy minimization: application to mesh adaptation. *Computer Methods in Applied Mechanics and Engineering*, 197(9-12): 1131–1146, 2008.
- J. Mosler and F. Cirak. A variational formulation for finite deformation wrinkling analysis of inelastic membranes. *Computer Methods in Applied Mechanics and Engineering*, 198(27-29):2087–2098, 2009.
- K. Nakashino and M. Natori. Three-dimensional analysis of wrinkled membranes using modification scheme of stress-strain tensor. *AIAA journal*, 44(7):1498–1504, 2006.
- K. Nakashino and M. C. Natori. Efficient modification scheme of stress-strain tensor for wrinkled membranes. *AIAA Journal*, 43(1):206–215, 2005.
- K. Nakashino, A. Nordmark, and A. Eriksson. Geometrically nonlinear isogeometric analysis of a partly wrinkled membrane structure. *Computers & Structures*, 239:106302, 2020.
- O. K. Nilsen. Simulation of crack propagation using isogeometric analysis applied with nurbs and lr b-splines. Master’s thesis, Institutt for matematiske fag, 2012.
- L. Piegl and W. Tiller. *The NURBS book*. Springer Science & Business Media, 1996.
- A. C. Pipkin. The relaxed energy density for isotropic elastic membranes. *IMA journal of applied mathematics*, 36(1):85–99, 1986.

- E. Puntel, L. Deseri, and E. Fried. Wrinkling of a stretched thin sheet. *Journal of Elasticity*, 105:137–170, 2011.
- T. Raible, K. Tegeler, S. Löhnert, and P. Wriggers. Development of a wrinkling algorithm for orthotropic membrane materials. *Computer methods in applied mechanics and engineering*, 194(21-24):2550–2568, 2005.
- E. Reissner. On tension field theory. *Proc. of the 5th Int. Congr. for Applied Mechanics Harvard Univ. & MIT*, pages 88–92, 1938.
- D. G. Roddeman, J. Drukker, C. W. J. Oomens, and J. D. Janssen. The wrinkling of thin membranes: part i—theory. *Journal of Applied Mechanics*, 54(4):884–887, 12 1987a.
- D. G. Roddeman, J. Drukker, C. W. J. Oomens, and J. D. Janssen. The wrinkling of thin membranes: Part ii—numerical analysis. *Journal of Applied Mechanics*, 54(4):888–892, 12 1987b.
- D. F. Rogers. *An introduction to NURBS: with historical perspective*. Morgan Kaufmann, 2001.
- R. Rossi, M. Lazzari, R. Vitaliani, and E. Oñate. Simulation of light-weight membrane structures by wrinkling model. *International Journal for Numerical Methods in Engineering*, 62(15):2127–2153, 2005.
- H. Schoop, L. Taenzer, and J. Hornig. Wrinkling of nonlinear membranes. *Computational Mechanics*, 29:68–74, 2002.
- D. Steigmann. Tension-field theory. *Proceedings of the Royal Society of London. A. Mathematical and Physical Sciences*, 429(1876):141–173, 1990.

- M. Stein and J. M. Hedgepeth. *Analysis of partly wrinkled membranes*. National Aeronautics and Space Administration, 1961.
- M. Taylor, K. Bertoldi, and D. J. Steigmann. Spatial resolution of wrinkle patterns in thin elastic sheets at finite strain. *Journal of the Mechanics and Physics of Solids*, 62:163–180, 2014.
- H. M. Verhelst, M. Möller, J. Den Besten, A. Mantzaflaris, and M. L. Kaminski. Stretch-based hyperelastic material formulations for isogeometric kirchhoff–love shells with application to wrinkling. *Computer-Aided Design*, 139:103075, 2021.
- H. Wagner. Flat sheet metal girders with very thin metal web. part i: general theories and assumptions. Technical report, 1931.
- X. Wang, J. Ma, S.-s. Law, and Q. Yang. Numerical analysis of wrinkle-influencing factors of thin membranes. *International Journal of Solids and Structures*, 97:458–474, 2016.
- X. F. Wang, Q. S. Yang, and S.-s. Law. Wrinkled membrane element based on the wrinkling potential. *International Journal of Solids and Structures*, 51(21-22):3532–3548, 2014.
- W. Wong and S. Pellegrino. Wrinkled membranes i: experiments. *Journal of Mechanics of Materials and Structures*, 1(1):3–25, 2006a.
- W. Wong and S. Pellegrino. Wrinkled membranes ii: analytical models. *Journal of Mechanics of Materials and Structures*, 1(1):27–61, 2006b.

- W. Wong and S. Pellegrino. Wrinkled membranes iii: numerical simulations. *Journal of Mechanics of Materials and Structures*, 1(1):63–95, 2006c.
- K. Woo, H. Igawa, and C. Jenkins. Analysis of wrinkling behavior of anisotropic membrane. *Computer Modeling in Engineering and Sciences*, 6:397–408, 2004.
- C. H. Wu. Nonlinear wrinkling of nonlinear membranes of revolution. *Journal of Applied Mechanics, Transactions ASME*, 45(3):533–538, 1978.
- C. H. Wu and T. R. Canfield. Wrinkling in finite plane-stress theory. *Quarterly of Applied Mathematics*, 39(2):179–199, 1981.